Journal of Alloys and Compounds 512 (2012) 23–26

Contents lists available at SciVerse ScienceDirect

Journal of Alloys and Compounds

journal homepage: www.elsevier.com/locate/jallcom

Mesoporous (N, S)-codoped TiO_2 nanoparticles as effective photoanode for dye-sensitized solar cells

Yuanyuan Li[a], Lichao Jia[a], Congcong Wu[a], Song Han[b], Yingpeng Gong[a], Bo Chi[a,*], Jian Pu[a], Li Jian[a]

[a] School of Materials Science and Engineering, State Key Lab of Material Processing and Die & Mould Technology, Huazhong University of Science and Technology, Wuhan 430074, China

[b] College of Forestry, Northeast Forestry University, Harbin 150040, China

ARTICLE INFO

Article history:
Received 18 June 2011
Received in revised form 18 August 2011
Accepted 19 August 2011
Available online 22 September 2011

Keywords:
Dye-sensitized solar cells
Codoping
Titania
Mesoporous nanoparticles

ABSTRACT

(N, S)-codoped titania (TiO_2) is synthesized by a simple template-free solvothermal method as photoanode for dye-sensitized solar cells (DSSCs). The results confirm that N and S have been doped into the lattice of anatase, which can enhance the visible-light absorbance and promote the electron transportation in TiO_2. The prepared (N, S)-codoped TiO_2 exhibits pure anatase phase mesoporous nanoparticles with average diameter of 60 nm. Mixing (N, S)-codoped TiO_2 with Degussa P25 as photoanode results in the improvement of open-circuit voltage and short-circuit photocurrent density of DSSC. And the corresponding DSSC obtains a high conversion efficiency of 8.0%.

1. Introduction

Dye-sensitized solar cell (DSSC), which has the advantages of low cost, simple preparation procedure, and relatively high energy-conversion efficiencies, has become the research focus of the new energy field [1–4]. Nanostructured TiO_2 could provide rapid electron transportation, large surface area for adsorption of dye molecules, and close electrical contact with the redox electrolyte and has been considered as a favorable material for the photoanode application for DSSC [5–7]. However, pure anatase shows photocatalytic activity only under ultraviolet light irradiation due to its wide band gap (3.2 eV), which leads to a low solar energy utilization. Many attempts have been made to improve the photocatalytic performance of TiO_2 photoanode for DSSCs by doping non-metal elements such as N, C and S [8–10]. For the N-doped TiO_2 photoanodes, improvement of both the open circuit voltage and the visible absorption [8], have been reported and high conversion efficiency has been recorded. In addition, the enhanced electron lifetime and great stability for N-doped TiO_2 DSSCs has been observed [11,12]. It has been suggested that doping TiO_2 with nonmetal elements such as N, C, and S can lead to the significant red-shift of the optical absorption edge [13–19]. Latest researches show that different ions codoping into TiO_2 can further enhance its photocatalytic activity [20]. The previous researches [21–23] indicated that (N, S)-codoped TiO_2 can greatly improve the photocatalytic activity of TiO_2 under visible light irradiation due to the hybridization of the introduced N 2p and S 3p, which could also promote the transportation of photogenerated electrons in TiO_2. However, to the best of our knowledge, there is no detailed research on (N, S)-codoped TiO_2 used as photoanode for DSSCs up to now.

In this paper, we synthesized (N, S)-codoped mesoporous TiO_2 (NST) nanoparticles by a simple template-free solvothermal method using thiourea as the sources of the nitrogen and sulfur, and then applied it as photoanode for DSSC. The mesoporous NST nanoparticles were mixed with Degussa P25 as photoanode and their performance in DSSC were evaluated. The improvement of the visible-light absorbance and the high specific surface area of this novel combined photoanode with mesoporous nanoparticles contribute to the increase of the performance of DSSC.

2. Experimental

2.1. Synthesis of (N, S)-codoped TiO_2 nanoparticles

(N, S)-codoped TiO_2 (NST) nanoparticles were prepared by a simple solvothermal method. In a typical synthesis process, 0.003 mol thiourea was firstly dissolved in 30 mL ethanol. Subsequently, the solution was added dropwise to a mixture of 0.003 mol tetra-butyl orthotitanate (TBOT) and 4 g HCl (37 wt%) under stirring at room temperature. After 120 min of stirring, the obtained transparent mixture was transferred into the Teflon-lined autoclave and heated at 150 °C for 6 h. Then the resultant mixture was washed with ethanol and separated by centrifugation three times to collect a white precipitate. Finally, the samples were obtained by annealing at 450 °C for 2 h. For comparison, undoped pure TiO_2 nanoparticles were also synthesized by removing thiourea during the synthesis process, and named NST0.

* Corresponding author. Tel.: +86 27 8755 8142; fax: +86 27 8755 8142.
E-mail address: chibo@hust.edu.cn (B. Chi).

0925-8388/$ – see front matter © 2011 Elsevier B.V. All rights reserved.
doi:10.1016/j.jallcom.2011.08.072

Table 1
Composition (wt%) of various TiO_2 cells.

Type of cells	NST particles	Degussa P25
1	0	100
2	5	95
3	10	90
4	20	80
5	100	0

2.2. Fabrication of photoanodes

TiO_2 photoanode films were fabricated on the fluorine-doped SnO_2 glass substrate (FTO, 10 $\Omega\,\square^{-1}$) by a doctor-blade method. In order to optimize the constituent, NST particles and Degussa P25 TiO_2 were mixed at different weight ratio to prepare various TiO_2 photoanodes. The ratios of each TiO_2 photoanode are listed in Table 1. TiO_2 particles were dispersed in α-terpineol as solvent and ethyl cellulose as binder. The photoanodes were obtained by calcination the coated combined TiO_2 films at 450 °C for 30 min.

2.3. Photovoltaic measurements

The photoanodes were immersed in an acetonitrile and tertbutanol (1:1) solution with 5 mM N719 (Solaronix SA, Switzerland) dye for 12 h to adsorb dye molecules. Pt counter electrodes were produced by coating H_2PtCl_6 solution onto FTO glass and sintered at 450 °C for 60 min. The redox electrolyte was composed of 0.3 M LiI, 0.05 M I_2, 0.3 M DMPII and 0.5 M TBP in acetonitrile. Photovoltaic performances were measured under a simulated AM1.5 solar source (CHF-XM500W, Beijing Trusttech Co. Ltd., China). Photocurrent voltage curves and impedance spectra were obtained from the electrochemical workstation (Solartron S1 1287–1260).

2.4. Characterization

The crystal phases of synthesized TiO_2 nanoparticles were determined by X-ray diffractometer (XRD) with a Cu Kα radiation. The binding energy (BE) of NST was measured by X-ray photoelectron spectroscopy (XPS). The microstructure was detected by the field emission scanning electron microscopy (FESEM). The absorption spectra of the photoanodes were recorded with the UV–vis spectrophotometer.

3. Results and analysis

Fig. 1 illustrates the XRD patterns of the NST and NST0 samples. It could be found that NST sample exhibits homogenous pure anatase phase, while the NST0 sample contains both the anatase and rutile phase. Normally, anatase titania is more capable of converting solar energy than rutile titania as the photoanode for DSSC. The results confirm that in the procedure for TiO_2 synthesis, doping may result in the formation of pure anatase rather than the mixture of anatase and rutile phase. Fig. 2a shows the morphology of the as-prepared NST particles. The particles are relatively presenting a spherical morphology with a diameter of approximately 60 nm. Fig. 2b exhibits the cross-sectional view of cell 3, which contains 10 wt% NST and 90 wt% P25. It indicates a mixture

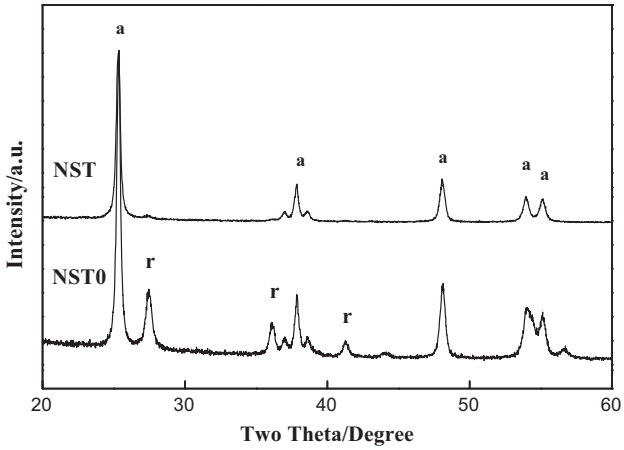

Fig. 1. XRD patterns of the NST and NST0 nanoparticles.

of TiO_2 nanoparticles with different sizes, where the smaller ones are P25 of particle size 25 nm and the larger are NST about 60 nm. This hierarchical particle size distribution would enable the more surface area and routes for electrons transportation. Furthermore, Fig. 3 shows the typical nitrogen adsorption–desorption isotherm of the as-prepared NST sample, which is a type IV isotherm curve with H2 hysteresis loop, the characteristic of mesoporous materials [13,24,25]. The inset of Fig. 3 is the corresponding BJH result about the pore size distribution. It confirms that the high specific surface area of NST is due to its mesoporous particle structure. The corresponding BJH result confirms that the pore size of NST is about 13.7 nm and BET surface area is 68.2 m^2/g. Thus, the cell with mesoporous nanoparticles and hierarchical structure would provide sufficient surface area rendering the photoanode high light harvesting through adsorbing more dye molecules on the TiO_2 surface.

To investigate the existence of N and S in doped TiO_2, the XPS spectra of NST, N 1s and S 2p are shown in Fig. 4. The peak for N 1s appears clearly at a BE of 398.9 eV, as shown in Fig. 4c, which refers to N species substitute for O atoms in the anatase TiO_2 lattice according to the relative researches [26,27], providing an N 2p state just above the valence band. Fig. 4b shows the S 2p peak at around 168.3 eV. Researches [28,29] have indicated that S 2p peaks are found for high oxidation states at BE > 168 eV. Thus these two BE peaks can be attributed to S^{6+} in the lattice replace for Ti^{4+}, meaning the S cationic doping in the lattice. It is also due to SO_4^{2-} ions on TiO_2 forming bidentate linkages with Ti^{4+} ions [26,30]. According

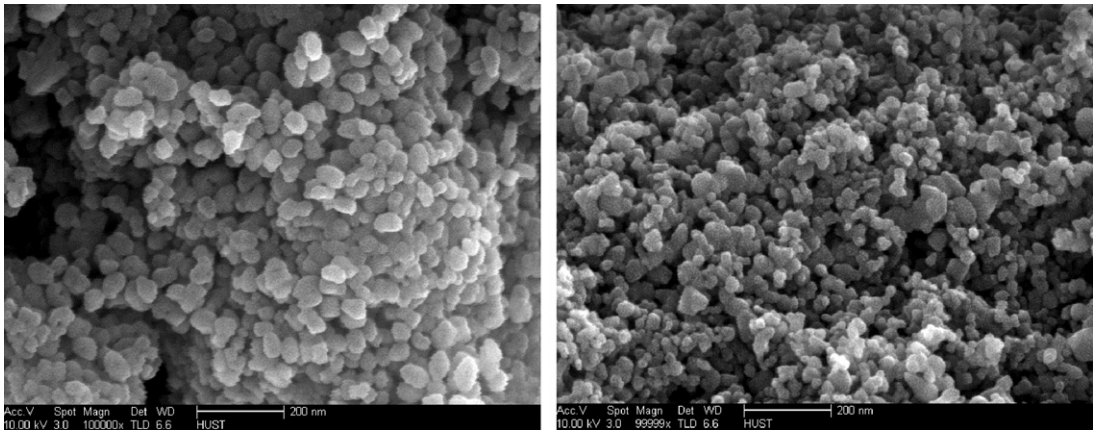

Fig. 2. FESEM micrograph of (a) NST particles, (b) cross-sectional view of cell 3.

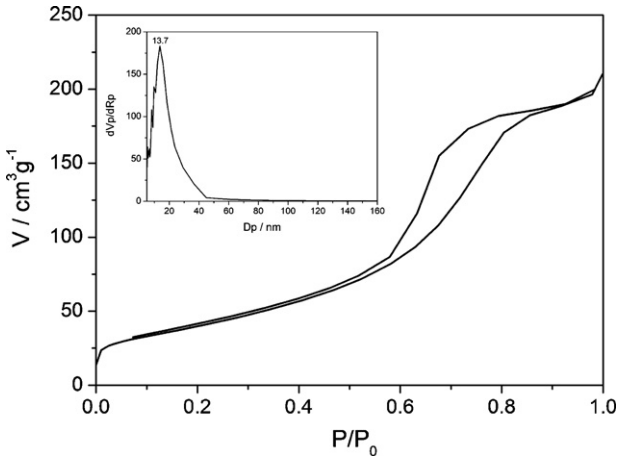

Fig. 3. A typical N_2 adsorption–desorption isotherm curve for NST. The inset: BJH result.

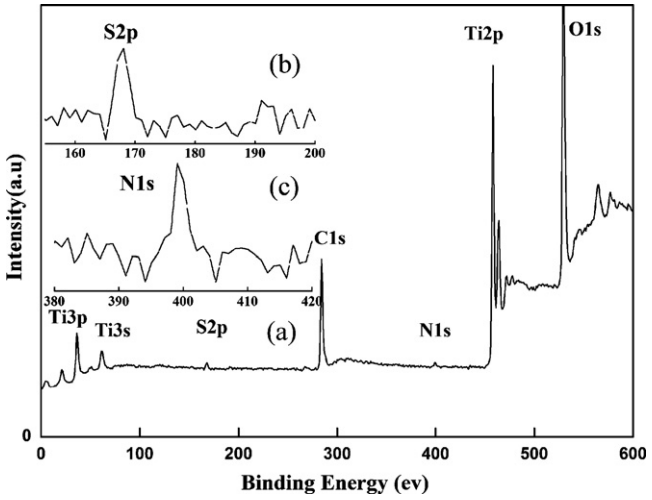

Fig. 4. The XPS spectra of (a) the NST nanoparticles, (b) S 2p, and (c) N 1s.

to the XPS analysis result, the content of N, S element is 0.62 at% and 0.35 at%, respectively.

I–V curves of the assembled cells based on the as-prepared mesoporous TiO_2 nanoparticles and commercial Degussa P25 photoanode are shown in Fig. 5, of which the effective areas are 0.25 cm^2. The measured open-circuit voltage (V_{oc}), short-circuit photocurrent density (J_{sc}), fill factor (FF), and light-to-electric conversion efficiencies (η) are listed in Table 2. Compared to the pure undoped TiO_2 (NST0) photoanode, (N, S)-codoped TiO_2 (NST cell 5) photoanode can remarkably improve J_{sc} from 8.98 to 10.01 mA cm^{-2}, FF from 0.50 to 0.55, and η from 3.3% to 4.0% simultaneously, though V_{oc} for the two photoanodes is almost similar. The improvement may be related with the following two factors. One refers to the fact that (N, S)-codoped anatase NST is more beneficial than undoped NST0 containing little rutile phase in DSSC, the other is that S and N codoping could greatly improve the light absorption of TiO_2 under visible light irradiation as depicted in the UV–vis absorption spectra (Fig. 6). The improvement of the visible-light absorbance may increase the number of photo-generated electrons and holes to participate into the photocatalytic reaction, which can enhance the performance of the DSSC. For comparison, photoanode with pure P25 is also shown in Table 2 (cell 1). It could be found that NST photoanode shows a little worse property than P25 photoanode, which may be due to the smaller particle size and higher specific surface areas of P25.

Table 2
Photovoltaic performance of dye-sensitized solar cells based on each cell.

Cell	V_{oc} (V)	J_{sc} (mA cm^{-2})	FF (%)	η (%)
1	0.749	12.59	62.56	5.9
2	0.820	18.2	46.23	6.9
3	0.822	19.00	51.22	8.0
4	0.836	13.85	40.59	4.7
5	0.724	10.01	55.19	4.0
NST0	0.733	8.98	50.13	3.3

An interesting result is that photoanode with the mixture of NST with P25 in ratio would enhance the performance of DSSCs effectively compared to the pure NST or P25 photoanode. Table 2 shows the performance of DSSCs with different photoanode composition of NST and P25 ratio. Generally, DSSCs with photoanode of the mixtures with NST and P25 have the enhanced performance. A sharp increase of V_{oc} and J_{sc} are observed with the sacrifice of fill factor on cell 2, 3, and 4 that have mixture photoanode of NST and P25, compared with cell 1 or 5. For the mixture photoanodes, the ratio of NST and P25 is found to be crucial to optimize the properties of the cells. With the increase of NST content from 5 wt% to 20 wt%, the conversion efficiency first increases and reaches the peak in cell 3, then decreases. The best performance of these cells is achieved in cell 3 and the corresponding V_{oc}, J_{sc}, and FF of cell 3 are 0.822 V, 19.00 mA cm^{-2} and 0.512, respectively, yielding an overall conversion efficiency (η) of 8.0%, which is 35.6% higher than that of cell 1 with single pure P25. The unique mesoporous nanoparticles and reasonable hierarchical structure can both load large

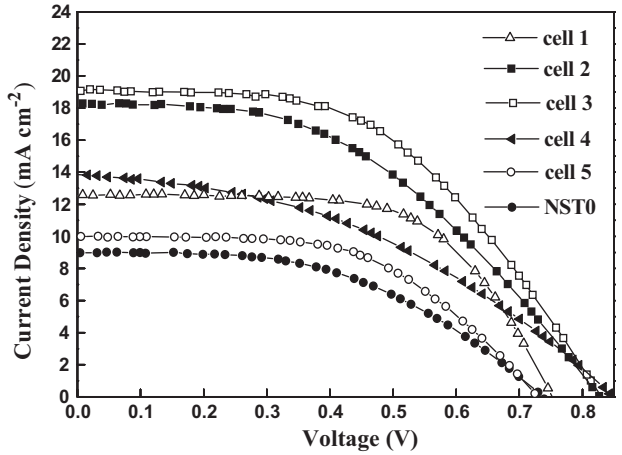

Fig. 5. *I–V* characteristics of DSSCs with different photoanodes.

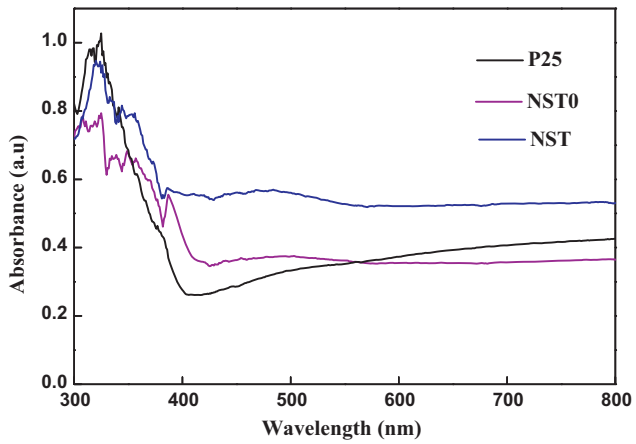

Fig. 6. UV–vis absorption spectra of P25, NST and NST0.

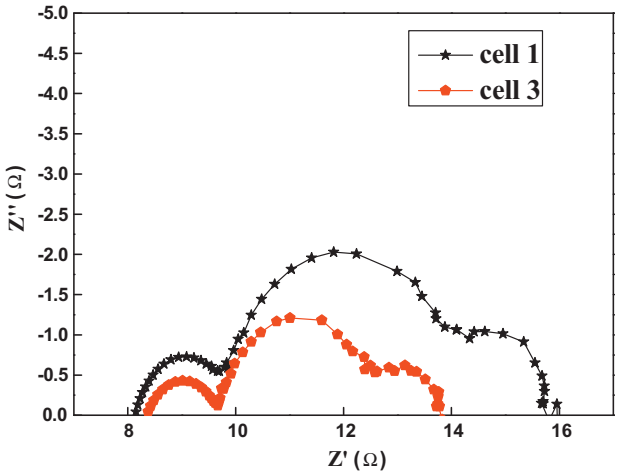

Fig. 7. EIS spectra of the DSSCs of cell 1 and cell 3.

amount of dye molecules and induce efficient electrolyte diffusions. Furthermore, the addition of NST nanoparticles offers a considerable improvement of the visible-light absorbance, resulting in more photo-generated electrons and holes to participate in the photocatalytic reaction. Moreover, the doping of N into the O lattice can not only increase the V_{oc} of DSSC, attributing to V_{fb} shifts to the negative direction appreciably, but also improve the J_{sc} by retarding the dye degradation, as proved in the reference [8]. Thus, the high efficiency observed on cell 3 is expectable.

To explore the difference in the interfacial characteristics of the photoanodes, electrochemical impedance spectroscopy (EIS) of the DSSCs was measured at an applied bias of V_{oc} and a frequency of range from 0.01 Hz to 1 MHz with AC amplitude of 10 mV at simulated AM1.5 solar light. Fig. 7 shows EIS of the cell 1 and cell 3. Three well-defined semicircles noted in the high region (>1 kHz), the middle region (1000–1 Hz) and the region of 1–0.1 Hz in both of the two EIS spectra are assigned to charge transfer processes occurring at the Pt/electrolyte interface and TiO_2/dye/electrolyte interface, within the electrolyte in Nernst diffusion respectively [31]. The resistance of cell 3 at the TiO_2/dye/electrolyte interface decreases to some extent over cell 1. The decreased resistance at the TiO_2/dye/electrolyte interface suggests that the diffusion of electrons in cell 3 is faster and more effective than that in cell 1, which is crucial to achieve a higher overall conversion efficiency. Usually the TiO_2/dye/electrolyte interface is significant as the interface controlling the photocurrent of the DSSC and the lower interfacial resistant is expected for high performance DSSC, which is consistent with the tendency of the observed J_{sc}. It is therefore demonstrated that the codoping of N and S could successfully accelerate the diffusion of electrons on the TiO_2 electrode and retard the charge recombination at the TiO_2/dye/electrolyte interface, which finally leads to an improvement of J_{sc}.

4. Conclusion

In summary, mesoporous (N, S)-codoped TiO_2 nanoparticles were successfully synthesized via a simple solvothermal method with the thiourea as the resources of N and S. The absorbance of visible-light of NST appears stronger than NST0 and P25. The DSSC composed with NST and reasonable ratio of P25 showed high overall performance with light-to-electric conversion efficiency of 8.0%, due to its hierarchical nanoparticle structure and high visible-light absorbance. The results confirm that (N, S)-codoped TiO_2 is proved to be a promising photoanode material for high performance DSSCs.

Acknowledgements

This research was financially supported by National Science Foundation of China under contract No. 50902056, Scientific Research Foundation for the Returned Overseas Chinese Scholars of Ministry of Education, Fundamental Research Funds for the Central Universities (HUST 2010MS087), and the State Key Lab of Material Processing and Die & Mould Technology. The authors would like to thank Materials Characterization Center of Huazhong University of Science and Technology for XRD, SEM and UV–vis assistance.

References

[1] O.B. Regan, M. Grätzel, Nature 353 (1991) 737–740.
[2] N.J. Cherepy, G.P. Smesad, M. Grätzel, J.Z. Zhang, J. Phys. Chem. B 101 (1997) 9342–9351.
[3] B. Chi, L. Zhao, J. Li, J. Pu, Y. Chen, C.C. Wu, T. Jin, J. Nanosci. Nanotechnol. 8 (2008) 3877–3882.
[4] G. Benk, P. Myllyperki, J. Pan, A.P. Yartsev, M. Sundstr, J. Am. Chem. Soc. 125 (2003) 1118–1119.
[5] Y.G. Kim, M.H. Lee, H.J. Kim, G. Lim, Y.S. Choi, N.G. Park, K. Kim, W.I. Lee, Adv. Mater. 21 (2009) 3668–3673.
[6] C.C. Wu, Y.J. Zhuo, P.N. Zhu, B. Chi, J. Pu, J. Li, J. Inorg. Mater. 24 (2009) 897–901.
[7] S.K. Dhungel, J.G. Park, Renew. Energy 35 (2010) 2776–2780.
[8] H.J. Tian, L.H. Hu, C.N. Zhang, W.Q. Liu, Y. Huang, L. Mo, L. Guo, J. Sheng, S.Y. Dai, J. Phys. Chem. C 114 (2010) 1627–1632.
[9] X.X. Wang, X.M. Song, G.Q. Wang, H.T. Wang, Q.G. Du, Micro Nano Lett. 5 (2010) 42–48.
[10] T. Hoshikawa, T. Ikebe, M. Yamada, R. Kikuchi, K. Eguchi, J. Photochem. Photobiol. A: Chem. 184 (2006) 78–85.
[11] T. Ma, M. Akiyama, E. Abe, I. Imai, Nano Lett. 5 (2005) 2543–2547.
[12] T. Lindgren, J.M. Mwabora, E. Avendaño, J. Jonsson, A. Hoel, C.G. Granqvist, S.E. Lindquist, J. Phys. Chem. B 107 (2003) 5709–5716.
[13] B. Chi, L. Zhao, T. Jin, J. Phys. Chem. C 111 (2007) 6189–6193.
[14] C. Karunakaran, A. Vijayabalan, G. Manikandan, P. Gomathisankar, Catal. Commun. 12 (2011) 826–829.
[15] K. Yang, Y. Dai, B.B. Huang, J. Phys. Chem. C 111 (2007) 18985–18994.
[16] L.C. Jia, C.C. Wu, Y.Y. Li, S. Han, Z.B. Li, B. Chi, J. Pu, J. Li, Appl. Phys. Lett. 98 (2011) 211903.
[17] G. Shao, J. Phys. Chem. C 113 (2009) 6800–6808.
[18] R. Asachi, T. Morikawa, T. Ohwaki, K. Aoki, Y. Taga, Science 293 (2001) 269–271.
[19] L.C. Jia, C.C. Wu, Y.Y. Li, S. Han, Z.B. Li, B. Chi, J. Pu, L. Jian, J. Alloy Compd. 509 (2011) 6067–6071.
[20] J.A. Rengifo Herrera, K. Pierzchała, A. Sienkiewicz, L. Forro, J. Kiwi, J.E. Moser, C. Pulgarin, J. Phys. Chem. C 114 (2010) 2717–2723.
[21] J.A. Rengifo-Herrera, C. Pulgarin, Sol. Energy 84 (2010) 37–43.
[22] J.H. Xu, J.X. Li, W.L. Dai, Y. Cao, H. Li, K.N. Fan, Appl. Catal. B: Environ. 79 (2008) 72–80.
[23] B. Naik, K.M. Parida, C.S. Gopinath, J. Phys. Chem. C 114 (2010) 19473–19482.
[24] F. Rouquerol, J. Rouquerol, K. Sing, Adsorption by Powders and Porous Solids, Academic Press, San Diego, 1999.
[25] K.S.W. Sing, D.H. Everett, R.A.W. Haul, L. Moscou, R.A. Pierotti, J. Rouquerol, T. Siemieniewska, Appl. Chem. 57 (1985) 603–619.
[26] M. Satish, B. Viswanathan, R.P. Viswanath, C.S. Gopinath, J. Nanosci. Nanotechnol. 9 (2009) 423–432.
[27] R. Bacsa, J. Kiwi, T. Ohno, P. Albers, V. Nadtochenko, J. Phys. Chem. B 109 (2005) 5994–6003.
[28] D.E. Gu, B.C. Yang, Y.D. Hu, Catal. Commun. 9 (2008) 1472–1476.
[29] F.Y. Wei, L.S. Ni, P. Cu, J. Hazard. Mater. 156 (2008) 135–140.
[30] T. Umebayashi, T. Yamaki, H. Itoh, K. Asai, Appl. Phys. Lett. 81 (2002) 454–456.
[31] C.P. Hsu, K.M. Lee, J.T.W. Huang, C.Y. Lin, C.H. Lee, L.P. Wang, S.Y. Tsai, K.C. Ho, Electrochim. Acta 53 (2008) 7514–7522.